Available online at www.sciencedirect.com

ScienceDirect

Energy Procedia 63 (2014) 7891 – 7912

Energy Procedia

GHGT-12

Numerical Simulation of Carbon Dioxide Injection in the Western Section of the Farnsworth Unit

M.D. White[a,]*, B.J. McPherson[b], R.B. Grigg[c], W. Ampomah[c], M.S. Appold[d]

[a]*Energy and Environment Directorate, Pacific Northwest National Laboratory, Richland, WA 99352, USA*
[b]*Energy and Geoscience Institute, University of Utah, Salt Lake City, UT 84108, USA*
[c]*Petroleum Recovery Research Center, New Mexico Tech, Socorro, NM 87801, USA*
[d]*Geological Sciences, University of Missouri, Columbia, MO 65211, USA*

Abstract

Numerical simulation is an invaluable analytical tool for scientists and engineers in making predictions about of the fate of carbon dioxide injected into deep geologic formations for long-term storage. Current numerical simulators for assessing storage in deep saline formations have capabilities for modeling strongly coupled processes involving multifluid flow, heat transfer, chemistry, and rock mechanics in geologic media. Except for moderate pressure conditions, numerical simulators for deep saline formations only require the tracking of two immiscible phases and a limited number of phase components, beyond those comprising the geochemical reactive system. The requirements for numerically simulating the utilization and storage of carbon dioxide in partially depleted petroleum reservoirs are more numerous than those for deep saline formations. The minimum number of immiscible phases increases to three, the number of phase components may easily increase fourfold, and the coupled processes of heat transfer, geochemistry, and geomechanics remain. Public and scientific confidence in the ability of numerical simulators used for carbon dioxide sequestration in deep saline formations has advanced via a natural progression of the simulators being proven against benchmark problems, code comparisons, laboratory-scale experiments, pilot-scale injections, and commercial-scale injections. This paper describes a new numerical simulator for the scientific investigation of carbon dioxide utilization and storage in partially depleted petroleum reservoirs, with an emphasis on its unique features for scientific investigations. The mathematical foundations of this new simulator for enhanced oil recovery are those of the simulators developed for carbon sequestration in deep saline reservoirs, altered to consider the increased number of potential phases and compositional aspects by considering the oil in the system. As a demonstration of the simulator, a numerical simulation of carbon dioxide utilization for enhanced oil recovery in the western section of the Farnsworth Unit, representing an early stage in the progression of numerical simulators for carbon utilization and storage in depleted oil reservoirs.

Peer-review under responsibility of the Organizing Committee of GHGT-12

* Corresponding author. Tel.: +1-509-372-6070; fax: +1-509-372-6089.
E-mail address: mark.white@pnnl.gov

Peer-review under responsibility of the Organizing Committee of GHGT-12
doi:10.1016/j.egypro.2014.11.825

Keywords: enhanced oil recovery; carbon sequestration; numerical simulation; Farnsworth Unit

1. Introduction

Many of the current numerical simulators for geologic sequestration in deep saline formations have undergone development and comparisons against internationally recognized computer codes, laboratory experiments, field trials, and commercial-scale injections over the last twelve years [1,2,3]. Such code validation activities will continue to provide new understanding of subsurface processes and increase scientific, regulatory, stakeholder, operator, and public confidence in the predictive capabilities of numerical simulation, especially in assessing the long-term fate of injected carbon dioxide.

The petroleum industry has been developing and applying numerical simulators to predict enhanced oil recovery with the injection of carbon dioxide into partially depleted reservoirs for more than 35 years [4,5]. The principal interest for these simulations has been to support economic assessments of new ventures and to make production forecasts. Over the last quarter century, advances in numerical simulators and processing have moved enhanced oil recovery applications from those using quarter symmetry on five-spot well patterns to multiple five-spot well patterns across a reservoir field. The last quarter century has additionally seen a shift in the numerical simulation industry, with simulation development capabilities being consolidated and migrating away from the oil companies proper [6,7,8,9]. The industrial numerical simulator market is competitive and the algorithms are generally proprietary. Competition in the market comes in part from the efficiency of the algorithms to compute phase conditions, compositions, and properties. More efficient equation-of-state (EOS) algorithms allow for larger computational domains and more complex petroleum compositions.

The Southwest Partnership on Carbon Sequestration (SWP), led by New Mexico Tech, recently started the commercial-scale injection phase (Phase III) of its U.S. Department of Energy (DOE) supported research project [10]. The emphasis of this phase of the project matches the change in focus for DOE supported Regional Carbon Partnership projects from deep saline formations to partially depleted oil and gas reservoirs. With the support and collaboration of Chaparral Energy of Oklahoma City [11], the SWP Phase III project will involve the injection of one million metric tons of carbon dioxide over five years into the Morrow sandstone in the western section of the Farnsworth Unit in the Texas panhandle. The key overall objectives of the project will be to monitor closely the injection and post-injection periods and to couple monitoring with numerical simulation to provide new understanding of both carbon utilization for enhanced oil recovery (EOR) processes, and carbon storage in depleted oil reservoirs which have undergone complex production operations. Injected carbon dioxide for the project has come from two anthropogenic sources since December 2010; Agrium's fertilizer plant in Borger, Texas, and the Arkalon ethanol plant in Liberal, Kansas.

A component of the SWP project is the development and application of a new numerical simulator for modeling carbon dioxide injection, utilization and storage in partially depleted oil and gas reservoirs. The new numerical simulator is a member of the STOMP suite of simulators, developed by the Pacific Northwest National Laboratory, which includes those for simulating carbon sequestration in deep saline formations. This new simulator, STOMP-EOR, is being developed as a scientific tool for investigating subsurface processes both during the injection (utilization) and post-injection periods (storage). The principal objective in developing the simulator has been to provide fully compositional, three-phase, and nonisothermal, geochemical, and geomechanical capabilities in a framework that promotes scientific discovery and understanding. The modular design of the simulator will allow researchers to investigate the impacts of complex processes such as wettability transitions, fluid entrapment, carbon dioxide miscibility, and phase relative permeability. A critical requirement for the simulator will be to have a numerically efficient EOS algorithm for its application to non-trivial computational domains.

Public and scientific confidence in the ability of numerical simulators used for carbon dioxide sequestration in deep saline formations has advanced via a natural progression of the simulators being proven against benchmark problems, code inter-comparisons, laboratory-scale experiments, pilot-scale injections, and commercial-scale injections. This paper documents the numerical simulation of the utilization of carbon dioxide for enhanced oil recovery in the western section of the Farnsworth Unit and represents an early stage in the progression of numerical simulators for carbon utilization and storage in depleted oil reservoirs. To understand ultimately the fate of carbon dioxide in oil reservoir environments requires proven numerical simulation capabilities for the injection period. The major challenges in matching numerical simulation results against those collected in the field will be fourfold: 1) the heterogeneous depositional environment of the Farnsworth Unit, 2) establishing initial conditions considering the historical primary and secondary recovery activities, 3) the unusually high minimum miscibility pressure of the Farnsworth oil, and 4) the alternating water and gas floods that will be implemented during the current recovery activities.

Nomenclature

a	cubic equation of state parameter (J m^3/$kmol^2$)
b	cubic equation of state parameter (m^3/kmol) or intermediate wetting function parameter
C	number of petroleum components
d	Peneloux volume shift parameter (m^3/kmol)
D	diffusion coefficient (m^2/s)
$\mathbf{E}$	energy flux vector (W/m^2)
$\mathbf{F}$	component flux vector (kg/s m^2)
g	acceleration of gravity (m/s^2)
h	enthalpy (J/kg) or capillary head (m)
$\mathbf{J}$	diffusive flux vector (kg/s m^2)
$\mathbf{k}$	intrinsic permeability tensor (m^2)
$\mathbf{k}_e$	effective thermal conductivity tensor (W/m K)
k_r	relative permeability
K^i	K-factor of component i
m	mass rate, kg/s or mass (kg) or van Genuchten function parameter
M	molecular weight (kg/kmol)
n	van Genuchten function parameter
$\mathbf{n}$	surface normal vector
P	pressure (Pa)
q_e	energy rate (W)
R	gas constant (8,314.4621 m^3 Pa/K kmol)
s	phase saturation
t	time (s)
T	temperature (˚C)
u	internal energy (J/kg)
v	molar volume (m^3/kmol)
$\mathbf{V}$	fluid flux vector (m/s)
V_n	volume of grid-cell n (m^3)
$\mathbf{z}$	gravitation unit vector
Z	compressibility factor
α	van Genuchten function parameter (m^{-1})
β	gas mole fraction
Γ_n	surface area of grid-cell n (m^2)

φ	fugacity coefficient
θ	contact angle (rad)
λ	Brooks and Corey function parameter
μ	dynamic viscosity (Pa s)
ρ	density (kg/m^3)
τ	tortuosity factor
ϕ	porosity
χ	mole fraction
ψ	total mass expressed as a mass fraction or Brooks and Corey function parameter (m)
ω	mass fraction or acentric factor

Subscripts

b	brine
c	critical
g	gas phase
l	aqueous phase
n	nonaqueous-liquid phase
r	residual or relative
t	total petroleum
γ	phase

Superscripts

i	component
mp	matching point
od	oven-dried

2. Mathematical Model

A new numerical simulator has been developed for scientific investigations of CO_2 utilization for enhanced oil recovery and sequestration in depleted petroleum reservoirs. This simulator, named STOMP-EOR, was designed to solve problems involving the production of oil and gas from petroleum reservoirs through the three stages of production primary, secondary, and tertiary recovery; where, tertiary recovery is principally by injection of CO_2 or flue gases with the potential for alternating water floods. This simulator is a member of the STOMP suite of numerical simulators and the name extension EOR signifies enhanced oil recovery. The simulator is founded on conservation equations for energy, water mass, salt mass, CO_2 mass, CH_4 mass, and a number of user-defined petroleum component masses that describe the transport of components through fluids and energy through geologic media. We assume three mobile fluids are possible: 1) aqueous, 2) nonaqueous-liquid and 3) gas. The aqueous phase primarily comprises water, with dissolved concentrations of CO_2 and salt. Dissolved concentrations of CH_4 and the petroleum components are optionally considered as being in low concentrations in the aqueous phase. The nonaqueous-liquid phase only comprises petroleum components, CO_2, and CH_4. Optionally the simulator can be operated in a black-oil mode; where, the governing conservation equations are reduced to four: 1) water mass, 2) oil mass, 3) gas mass, and 4) salt mass.

2.1. Conservation Equations

The conservation equations equate the change in the conserved quantity within a volume over time with the net flux of the conserved quantity into the volume across the volume surface plus any net source of the conserved quantity with the volume. For the energy equation the conserved quantity within a volume is formulated in terms of

phase internal energy; the fluxes of energy are by mobile phase advection and thermal diffusion; energy flux associated with component diffusive flux is ignored; and energy sources are either associated with mass sources or heat sources;

$$\frac{\partial}{\partial t}\int_{V_n}\left[\sum_{\gamma=l,n,g}\left(\phi\,\rho_\gamma\,s_\gamma\,u_\gamma\right)\right]dV_n=\int_{\Gamma_n}\left[\mathbf{E}\cdot\mathbf{n}\right]d\Gamma_n+\int_{V_n}\left[\sum_{\gamma=l,n,g}\left(h_\gamma\,m_\gamma\right)+q_e\right]dV_n \tag{1}$$

Heat flux is a combination of advective and conductive components;

$$\mathbf{E}=-\nabla\left(\mathbf{k}_e\,\nabla T\right)+\sum_{\gamma=l,n,g}\left(\rho_\gamma\,h_\gamma\,\mathbf{V}_\gamma\right) \tag{2}$$

Advective fluxes of the mobile phases are computed according to Darcy's law;

$$\mathbf{V}_\gamma=-\frac{k_{r\gamma}\,\mathbf{k}}{\mu_\gamma}\left(\nabla P_\gamma+\rho_\gamma\,g\,\mathbf{z}\right) \tag{3}$$

The conservation equations for water, CO_2, CH_4, salt and the user-defined petroleum component masses have a similar form and consider the migration of the conserved quantities via both diffusion and advection through the active mobile phases, where the superscript *i* refers to the conserved component;

$$\frac{\partial}{\partial t}\int_{V_n}\left[\sum_{\gamma=l,n,g}\left(\phi\,\rho_\gamma\,s_\gamma\,\omega_\gamma^i\right)\right]dV_n=\int_{\Gamma_n}\left[\mathbf{F}^i\cdot\mathbf{n}\right]d\Gamma_n+\int_{V_n}\left[\sum_{\gamma=l,n,g}\left(\omega_\gamma^i\,m_\gamma\right)\right]dV_n \tag{4}$$

Component flux is a combination of advective and conductive contributions;

$$\mathbf{F}^i=\sum_{\gamma=l,n,g}\left(\rho_\gamma\,\omega_\gamma^i\,\mathbf{V}_\gamma+\mathbf{J}_\gamma^i\right) \tag{5}$$

Diffusive fluxes of components through the mobile phases are computed from gradients in molar concentration, considering molecular diffusion, but ignoring hydraulic dispersion;

$$\mathbf{J}_\gamma^i=-\phi\,\rho_\gamma\,s_\gamma\,\frac{M^i}{M_\gamma}\left(\tau_\gamma\,D_\gamma^i\right)\nabla\chi_\gamma^i \tag{6}$$

2.2. Equation of State

In STOMP-EOR three mobile phases are considered: 1) aqueous, 2) nonaqueous-liquid, and 3) gas. Aqueous phase properties are considered to be a function of temperature, pressure, dissolved salt and dissolved CO_2 concentrations. CH_4 and the petroleum components are considered to be passive solutes in the aqueous phase. Dissolved salt and CO_2 concentrations are computed via the formulations of Spycher et al. [12] for temperatures below 100˚C and Spycher and Pruess [13] for temperatures above 100˚C, with corrections for dissolved salt provided in Spycher and Pruess [13]. The Spycher formulations are based on the Redlich-Kwong equation of state with parameters fitted from published experimental data for CO_2-H_2O systems. Adding salt to the mixture results in

lower amounts of CO_2 in the aqueous phase (i.e., salting out effect). Aqueous properties are generally calculated starting with the pure-water values computed as a function of temperature and pressure using the ASME steam table formulations [14].

Nonaqueous-liquid and gas properties are considered to be a function of temperature, pressure, and molar concentrations of CO_2, CH_4, and the user-defined petroleum components. Gas phase properties are additionally dependent on water vapor concentration. Cubic equations of state form the basis for determining the appearance and properties of the nonaqueous-liquid and gas phases depending on temperature, pressure, and total molar concentrations of the CO_2, CH_4, and the user-defined petroleum components. The current version of STOMP-EOR has two cubic equations of state implemented: 1) Peng-Robinson [15] and 2) Soave-Redlich-Kwong [16,17]. The Peng-Robinson (PR) [15] and Soave-Redlich-Kwong (SRK) [16,17] cubic equation of states can be expressed in a general format:

$$P = \frac{R\,T}{v - b} - \frac{a\left(T\right)}{\left(v + \delta_1\, b\right)\left(v + \delta_2\, b\right)} \tag{7}$$

where; the two delta terms are dependent on a single parameter c:

$$\delta_1 = \frac{1}{2}\left(c + 1 + \sqrt{\left(c+1\right)^2 + 4\,c}\right);\ \delta_2 = \frac{1}{2}\left(c + 1 - \sqrt{\left(c+1\right)^2 + 4\,c}\right) \tag{8}$$

For the SRK EOS c = 0 and for the PR-EOS c = 1. Departure from the ideal gas law can be expressed via the compressibility:

$$Z = \frac{P\,v}{R\,T} \tag{9}$$

Parameters a and b in Eqn. 1 can be related to critical properties and the Pitzer acentric factor. Mixtures are treated via mixing rules and binary interaction parameters. One flaw in the original forms of the cubic equations of state was their poor liquid density predictions. Peneloux [18] resolved this problem, without altering the phase equilibrium calculation by slightly altering the form of the cubic equation of state:

$$P = \frac{R\,T}{v - b} - \frac{a\left(T\right)}{\left(\left[v + d\right] + \delta_1\left[b + d\right]\right)\left(\left[v + d\right] + \delta_2\left[b + d\right]\right)} \tag{10}$$

By introducing a volume translation or volume shift parameter d, which also can be expressed in terms of critical properties and the Pitzer acentric factor. Oil and gas in petroleum reservoirs are complex mixtures of hundreds of components. As STOMP-EOR solves a mass conservation equation for each component, it is not computationally practical to include every component in the petroleum mixture in a STOMP-EOR simulation. The preferred approach is to combine individual petroleum fractions into petroleum components.

2.3. Phase Stability and Equilibrium

STOMP-EOR simultaneously solves conservation equations at each grid cell for thermal energy, water mass, CO_2 mass, CH_4 mass, salt mass, and petroleum component mass for each declared petroleum component. The energy equation can be removed from the solved equations, yielding an isothermal calculation. The CO_2, CH_4 and salt mass conservation equations are active by default, but can be removed from the suite of solved coupled

equations. Each solved equation has an associated primary variable for which a solution is sought. The primary variable set switches depending on the phase state and composition of the petroleum components. Five principal primary variable sets are used for the five principal phase states, with secondary switching of the primary variable and solved equation with petroleum component concentrations. A critical component of the EOS algorithms is the calculation of stable phases and the equilibrium of phases, when multiple phases occur. The current version of STOMP-EOR uses several core assumptions concerning phases. The aqueous phase is comprised only of liquid water, dissolved CO_2, and dissolved salt. The gas phase comprises petroleum components plus CO_2, CH_4, and water vapor. The nonaqueous-liquid phase comprises only petroleum components plus CO_2 and CH_4.

A critical calculation throughout the simulation is the determination of whether gas and nonaqueous-liquid phases exist, and if both exist what is the composition of the phases. Two principal assumptions are taken in making this calculation: 1) phase equilibrium between the gas and nonaqueous liquid phases occurs, and 2) aqueous phase is ignored. The simulator is designed such that the temperature, pressure, and mole fraction of the petroleum components, plus CO_2 and CH_4, are known. This calculation is referred to as the isothermal flash two-phase flash and its correct solution yields the global minimum in Gibbs energy. The procedure follows the techniques of Michelsen and Mollerup [19]. The first step is to estimate the equilibrium factors (i.e., K-factors) assuming both gas and nonaqueous-liquid phases occur, using the Wilson [20] approximation:

$$\ln\left(K^i\right)=\ln\left(\frac{P_c^i}{P}\right)+5.373\left(1+\omega^i\right)\left(1-\frac{T_c^i}{T}\right);\quad K^i=\frac{\chi_g^i}{\chi_n^i}=\frac{\varphi_n^i}{\varphi_g^i} \tag{11}$$

Given an initial guess to the K-factors, the mole fraction of gas (i.e., β) is computed using the Rachford-Rice equation [21]:

$$\sum_{i=1}^{C}\left(\chi_g^i-\chi_n^i\right)=\sum_{i=1}^{C}\chi_t^i\left[\frac{K^i-1}{1-\beta+\beta K^i}\right]=0 \tag{12}$$

A □ value of 1, indicates gas only, a □ value of 0, indicates nonaqueous-liquid only and an intermediate □ value, indicates two-phase conditions (i.e., gas and nonaqueous-liquid). The details of the solution algorithm are described in detail in Michelsen and Mollerup [19], and represent a career of publications by Michelsen, but essentially involve conducting phase stability analyses whenever □ is near 0 or 1, and isothermal flash calculations for more intermediate values. These calculations can be computationally expensive, and often represent a significant component in building the Jacobian matrix. The results from these calculations are the molar fractions and compositions of the gas and nonaqueous-liquid phases.

2.4. Solution Scheme

The governing equations and associated constitutive equations are solved numerically via temporal and spatial discretization. The equations are discretized in time using a backward Euler scheme, yielding a fully implicit solution for the primary unknowns at the new time step. Spatial discretization is via the finite volume formulation using a structured grid comprised of hexahedral cells. Nodes are located at the volumetric centroids of the hexahedral cells. Grids are constructed to be orthogonal, or nearly orthogonal, with the vector between cell centroids being aligned with intervening surface normals. Spatial and temporal discretization of the governing equations yields a set of nonlinear algebraic equations for each grid cell. Newton-Raphson iteration with numerical differentiation is employed to resolve the nonlinearities in the algebraic equations. The number of equations solved per grid cell equals 5 plus the number of user specified petroleum components for the compositional option and 4 for the black-oil option. For the compositional option, specifying isothermal conditions, isobrine conditions, or iso-

CO2 conditions can reduce this number. A primary variable is associated with each solved governing equation. The set of solved primary variables varies between grid cells depending on the phase state of the grid cell (i.e., primary variable switching). The primary variable switching scheme involves 5 phase conditions and a sub-switching scheme for assigning the system pressure to a conservation equation. The scheme is outlined in Table 1 and allows for aqueous, nonaqueous-liquid, and gas saturation conditions between 0.0 and 1.0, inclusive. Primary variable switching with phase condition transitions occurs between Newton-Raphson iterations, yielding the potential for phase condition flopping during a time step.

Table 1. Primary Variable Switching Scheme

Saturation State	Energy	Water Mass	Salt Mass	CO_2 Mass	CH_4 Mass	Petroleum Comp. Mass
$s_l = 1\ s_g = 0\ s_n = 0$	T	$P = P_l$	ψ_b^s	$P_v^{CO_2}$	$m_t^{CH_4}$	m_t^i
$0 < s_l < 1\ s_g = 0\ s_n > 0$	T	s_l	ψ_b^s	$P = P_n$ or $\chi_t^{CO_2}$	$P = P_n$ or $\chi_t^{CH_4}$	$P = P_n$ or χ_t^i
$0 < s_l < 1\ s_g > 0\ s_n > 0$	T	s_l	ψ_b^s	$P = P_g$ or $\chi_t^{CO_2}$	$P = P_g$ or $\chi_t^{CH_4}$	$P = P_g$ or χ_t^i
$s_l = 0\ s_g = 0\ s_n > 0$	T	s_l	m_t^s	$P = P_n$ or $\chi_t^{CO_2}$	$P = P_n$ or $\chi_t^{CH_4}$	$P = P_n$ or χ_t^i
$s_l = 0\ s_g > 0\ s_n > 0$	T	s_l	m_t^s	$P = P_g$ or $\chi_t^{CO_2}$	$P = P_g$ or $\chi_t^{CH_4}$	$P = P_g$ or χ_t^i

3. k-s-P Relationships

Fluids migrate through the subsurface in response to pressure gradients and buoyancy forces. Both pressure gradients and buoyancy forces are specific to the mobile fluid phases (e.g., gas phase migrates under the driving forces of gas pressure differences and gas density differences). Parameters that determine volumetric fluid flux rates given pressure and buoyancy driving forces are intrinsic permeability, phase viscosity, and phase relative permeability. Functions describing the relationships between phase saturations and phase pressure differences (i.e., s-P relationships) define local phase pressures and saturations within grid cells and pressure gradients between grid cells. Functions describing the relationship between phase relative permeability and phase saturations (i.e., k-s relationships) define the local relative permeabilities of mobile phases within grid cells.

3.1. Saturation versus Capillary Pressure

s-P relationships describe the relationship between interphase capillary pressure and phase saturation. STOMP-EOR is currently being developed as a three-phase simulator: 1) gas, 2) aqueous, and 3) nonaqueous-liquid. The liquid phases (i.e., aqueous and nonaqueous liquid) are assumed to wet the solid surfaces of the geologic media. The gas phase is assumed to be the nonwetting phase. The degree to which the solid surface is wet is controlled by the contact angle; where, the contact angle varies from 0˚ to 180˚. A contact angle of 0˚ indicates the system is aqueous wet (i.e., water wet) and a contact angle of 180˚ indicates a nonaqueous-liquid wet (i.e., oil wet) system. Mixed-wettability between the aqueous and nonaqueous phase occur at contact angles between 0˚ and 180˚. The s-P relationship in STOMP-EOR is used to calculate the phase capillary pressures from phase saturations, or in an inverse manner the phase saturations from phase capillary pressures. The primary variable set in STOMP-EOR uses phase saturations as unknowns, so the forward calculation will be from phase capillary saturations to phase capillary pressures.

The mixed-wet s-P relationships in STOMP-EOR use a base function, such as the van Genuchten function [22] or the Brooks and Corey function [23]. For a contact angle of 0˚ the base function is used in its original form, yielding a relationship between aqueous saturation and the nonaqueous-liquid to aqueous capillary head. This function is shown as the black line in Fig. 1, for an example Brooks and Corey base function [23]. In this plot the gas saturation is set to 0.0, yielding a total liquid saturation of 1.0. For a contact angle of 180˚ the base function is used in its original form, but with the negative of the nonaqueous-liquid to aqueous capillary head, yielding the nonaqueous-liquid saturation. The aqueous saturation is then computed from the difference in gas saturation and nonaqueous-liquid saturation. This function is shown as the purple line in Fig. 1.

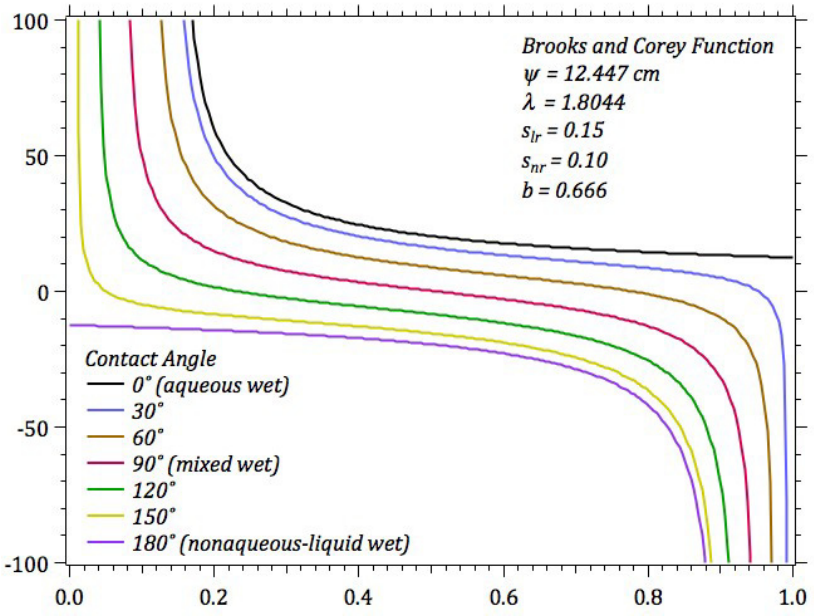

Fig. 1. Aqueous saturation versus capillary head using the Brooks and Corey function [23] with total-liquid saturation = 1.0

The total-liquid saturation is the sum of the aqueous and nonaqueous-liquid saturations and is a function of the capillary pressure between the gas and greater of the aqueous and nonaqueous-liquid pressure. The aqueous and nonaqueous saturations are functions of the total-liquid saturation and the nonaqueous-liquid to aqueous capillary pressure, which for mixed-wet systems can be positive or negative. Given the three phase saturations, the nonaqueous-liquid to aqueous capillary pressure is determined from contact-angle-scaled nonaqueous-liquid to aqueous and aqueous to nonaqueous-liquid indicial capillary heads:

$$h_{nl} = \left(\left(\frac{1+\cos\theta}{2} \right)^b \right) h^*_{nl} - \left(\left(\frac{1-\cos\theta}{2} \right)^b \right) h^*_{ln} \tag{13}$$

The "*b*" parameter is used to adjust the distribution of intermediate wetting curves between the aqueous-wet and nonaqueous-liquid wet limits. The indicial nonaqueous-liquid to aqueous capillary pressure is determined from the base s-P function, from the effective indicial aqueous saturation:

$$h_{nl}^{*} = \psi \left(\frac{1}{\overline{s}_l^{*}} \right)^{\left(\frac{1}{\lambda}\right)} \quad or \quad h_{nl}^{*} = \frac{\left(\left(\overline{s}_l^{*} \right)^{\left(-\frac{1}{m}\right)} - 1 \right)^{\left(\frac{1}{n}\right)}}{\alpha} \tag{14}$$

and the indicial aqueous to nonaqueous-liquid capillary pressure is determined from the base sP function, from the effective indicial nonaqueous-liquid saturation:

$$h_{ln}^{*} = \psi \left(\frac{1}{\overline{s}_n^{*}} \right)^{\left(\frac{1}{\lambda}\right)} \quad or \quad h_{ln}^{*} = \frac{\left(\left(\overline{s}_n^{*} \right)^{\left(-\frac{1}{m}\right)} - 1 \right)^{\left(\frac{1}{n}\right)}}{\alpha} \tag{15}$$

The effective indicial aqueous and nonaqueous-liquid saturations are determined from the indicial actual saturations and the indicial residual saturations; and the indicial actual aqueous and nonaqueous saturations are independent of the gas saturation:

$$\overline{s}_l^{*} = \frac{s_l^{*} - s_{lr}^{*}}{1 - s_{lr}^{*}}; \; \overline{s}_n^{*} = \frac{s_n^{*} - s_{nr}^{*}}{1 - s_{nr}^{*}}; \; s_l^{*} = \frac{s_l}{s_l + s_n}; \; s_n^{*} = \frac{s_n}{s_l + s_n} \tag{16}$$

The indicial residual aqueous and nonaqueous saturations are determined from contact-angle-scaled actual residual saturations:

$$s_{lr}^{*} = s_{lr} \left(\frac{1 + \cos\theta}{2} \right); \; s_{nr}^{*} = s_{nr} \left(\frac{1 - \cos\theta}{2} \right) \tag{17}$$

3.2. Extension below Residual Saturation

s-P Functions describe the relationship between interphase capillary pressure and phase saturation. The liquid phases (i.e., aqueous and nonaqueous liquid) are assumed wet the solid surfaces of the geologic media. The gas phase is assumed to be the nonwetting phase. The injection of CO_2 into a reservoir has the potential of forcing the total-liquid saturation below the residual saturation. Conventional capillary pressure and saturation functions are limited to saturations above the residual saturation. For these functions, the capillary pressure tends toward infinity as the aqueous saturation approaches the residual saturation. This limitation can be overcome by specifying an extension option for the either the van Genuchten [22] or Brooks and Corey [23] characteristic functions. The Webb [24] extension divides the capillary pressure-saturation function into two regimes. For low aqueous saturation the function follows a logarithmic form, and for moderate to high saturations the function follows the specified form (e.g., van Genuchten [22], Brooks and Corey [23]). Transition between the two forms occurs at the matching point, which occurs at the point where the two functions have matching slopes. The low-saturation function is a linear function on a semi-log plot:

$$s = \frac{\log\left(\frac{h}{h^{mp}}\right)}{\gamma} + s^{mp}; \quad \gamma = -\frac{\log\left(\frac{h_{od}}{h^{mp}}\right)}{s^{mp}} \tag{18}$$

The matching point saturation and capillary pressure head is determined by setting the partial derivative of the aqueous saturation with respect to the capillary pressure head in Webb equation equal to the partial derivative of the aqueous saturation with respect to the capillary pressure head in the specified function form (e.g., van Genuchten [22] or Brooks and Corey [23]), setting the capillary pressure head to the matching point capillary pressure head, setting the aqueous saturation to the matching point aqueous saturation and solving for the matching point aqueous saturation. A nonlinear solve is required to determine the matching point saturation and capillary pressure head for the van Genuchten [22] or Brooks and Corey [23] functions, but this solution is only required once, during simulation initialization. An oven-dried head of 10^9 Pa (~105 m) is used for the Webb [24] extension model.

For a gas-nonaqueous liquid-aqueous mixed-wet system three matching point saturations and heads are required: 1) gas-total liquid, 2) nonaqueous liquid-aqueous, and 3) aqueous-nonaqueous liquid. The s-P curves are divided into two components. Below the matching-point saturation or above the matching-point head the Webb [24] extension is used. Conversely above the matching-point saturation or below the matching-point head the conventional base function is used. The form of the Webb [24] extension provides for a smooth transition across the matching-point. For the mixed-wet system the head-shifted actual aqueous saturation is computed from either the base s-P function or Webb [24] extension, using a contact-angle shifted nonaqueous-liquid to aqueous capillary head.

$$\begin{aligned} &if\left(h_{nl}^{*} > h_{nl}^{mp}\right)\ s_l^{*} = \frac{\log\left(\frac{h_{od}}{h_{nl}^{*}}\right)}{\gamma_{nl}}; \gamma_{nl} = \frac{s_l^{mp}}{\log\left(\frac{h_{od}}{h_{nl}^{mp}}\right)} \\ &if\left(h_{nl}^{*} \le h_{nl}^{mp}\right)\ s_l^{*} = \bar{s}_l^{*}\left(1 - s_{lr}^{*} - s_{nr}^{*}\right) + s_{lr}^{*};\ \bar{s}_l^{*} = \left[1 + \left(\alpha\, h_{nl}^{*}\right)^{n}\right]^{-m} \text{ or } \bar{s}_l^{*} = \left[\frac{\psi}{h_{nl}^{*}}\right]^{\lambda} \end{aligned} \tag{19}$$

The head-shifted actual nonaqueous-liquid saturation is computed from either the base s-P function or Webb [24] extension, using a contact-angle shifted aqueous to nonaqueous-liquid capillary head.

$$\begin{aligned} &if\left(h_{ln}^{*} > h_{ln}^{mp}\right)\ s_n^{*} = \frac{\log\left(\frac{h_{od}}{h_{ln}^{*}}\right)}{\gamma_{ln}}; \gamma_{ln} = \frac{s_n^{mp}}{\log\left(\frac{h_{od}}{h_{ln}^{mp}}\right)} \\ &if\left(h_{ln}^{*} \le h_{ln}^{mp}\right)\ s_n^{*} = \bar{s}_n^{*}\left(1 - s_{lr}^{*} - s_{nr}^{*}\right) + s_{nr}^{*};\ \bar{s}_n^{*} = \left[1 + \left(\alpha\, h_{ln}^{*}\right)^{n}\right]^{-m} \text{ or } \bar{s}_n = \left[\frac{\psi}{h_{ln}^{*}}\right]^{\lambda} \end{aligned} \tag{20}$$

The actual total-liquid saturation is computed from the base s-P function or Webb [24] extension, using the gas to total-liquid capillary head; where, the total-liquid pressure is the maximum of the aqueous and nonaqueous-liquid pressure.

$$if\left(h_{gt}^{*} > h_{gt}^{mp}\right)\ s_t = \frac{\log\left(\frac{h_{od}}{h_{gt}^{*}}\right)}{\gamma_{gt}};\gamma_{gt} = \frac{s_t^{mp}}{\log\left(\frac{h_{od}}{h_{gt}^{mp}}\right)} \qquad (21)$$

$$if\left(h_{gt}^{*} \le h_{gt}^{mp}\right)\ s_t = \overline{s}_t\left(1 - s_{lr}^{*} - s_{nr}^{*}\right) + s_{lr}^{*} + s_{nr}^{*};\ \overline{s}_t = \left[1 + \left(\alpha\, h_{gt}^{*}\right)^{n}\right]^{-m} \text{ or } \overline{s}_t = \left[\frac{\psi}{h_{gt}^{*}}\right]^{\lambda}$$

An example of the Webb [24] extension applied in conjunction with the Brooks and Corey [23] base functions for a mixed-wet system are shown in Fig. 2.

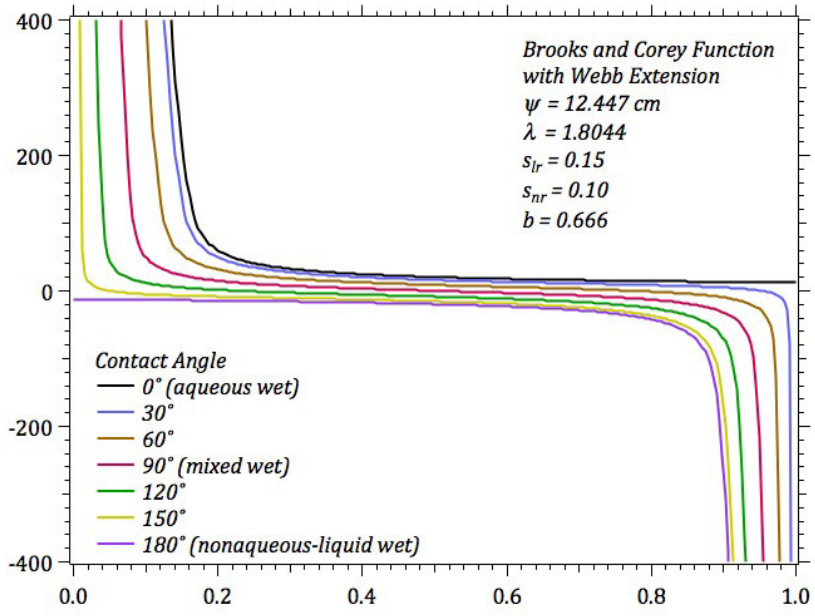

Fig. 2. Aqueous saturation versus capillary head using the Brooks and Corey function [23] with total-liquid saturation = 1.0

3.3. Relative Permeability versus Saturation

STOMP-EOR considers three mobile phases: 1) aqueous, 2) nonaqueous-liquid, and 3) gas, each with a unique relative permeability. Relative permeability often varies by orders of magnitude with saturation and often is the most nonlinear component of the governing equations and constitutive relationships. For carbon sequestration in deep saline reservoirs the relative permeability of the supercritical CO_2-rich phase has been shown to a critical parameter for predicting formation injectivity and the fate of injected CO_2 [25,26]. A similar situation occurs for petroleum reservoirs; where, there is the potential for three or occasionally four relative permeability functions, but the situation is complicated by the potential for miscibility of the injected CO_2 with the oil under reservoir pressure and temperature conditions. The classical approach for predicting relative permeabilities for petroleum reservoirs is to combine binary (aqueous - nonaqueous liquid (i.e., oil-water); and nonaqueous liquid-gas (i.e., oil-gas) relative permeability relationships to yield three-phase relative permeabilities (aqueous, nonaqueous-liquid, and gas). Stone-

I [27], Stone-II [28], and Baker [29] combination models are common approaches and currently implemented in STOMP-EOR.

Mixtures of petroleum components and CO_2 have complex phase diagrams that depend the mixture composition, which can vary across the petroleum reservoir with the injection of CO_2. A typical phase envelope diagram is shown in Fig. 3. When temperature and pressure conditions are above the bubble-point branch and the temperature is below the critical point, liquid conditions occur and the pore space will be filled with aqueous and nonaqueous liquid, requiring determination of aqueous and nonaqueous-liquid relative permeability. Conversely, when temperature and pressure conditions are in the gas region and the pressure is below the critical point, gas conditions occur (i.e., gas and aqueous relative permeability). When temperature and pressure conditions are within the phase envelope liquid and gas conditions occur, yielding the potential for aqueous, nonaqueous-liquid, and gas phases occurring simultaneously in the pore space. Uncertainty about the state of the petroleum component-rich phase, however, arises when the temperature and pressure conditions are outside of the two-phase region between the liquid and gas regions. In this region the petroleum-component-rich phase has properties that are intermediate between liquid and gas, its unclear as to what the relative permeability of the phase should be. This situation arises with the injection of CO_2 for enhanced oil recovery, when the reservoir pressure is maintained above the minimum miscibility pressure. There clearly is opportunity here for gaining a more scientific understanding of relative permeability of the petroleum-component-rich phase in this region of the phase envelope. STOMP-EOR currently assumes a linear transition across this region of the phase envelope, using nonaqueous liquid and gas saturations as the transitioning parameter.

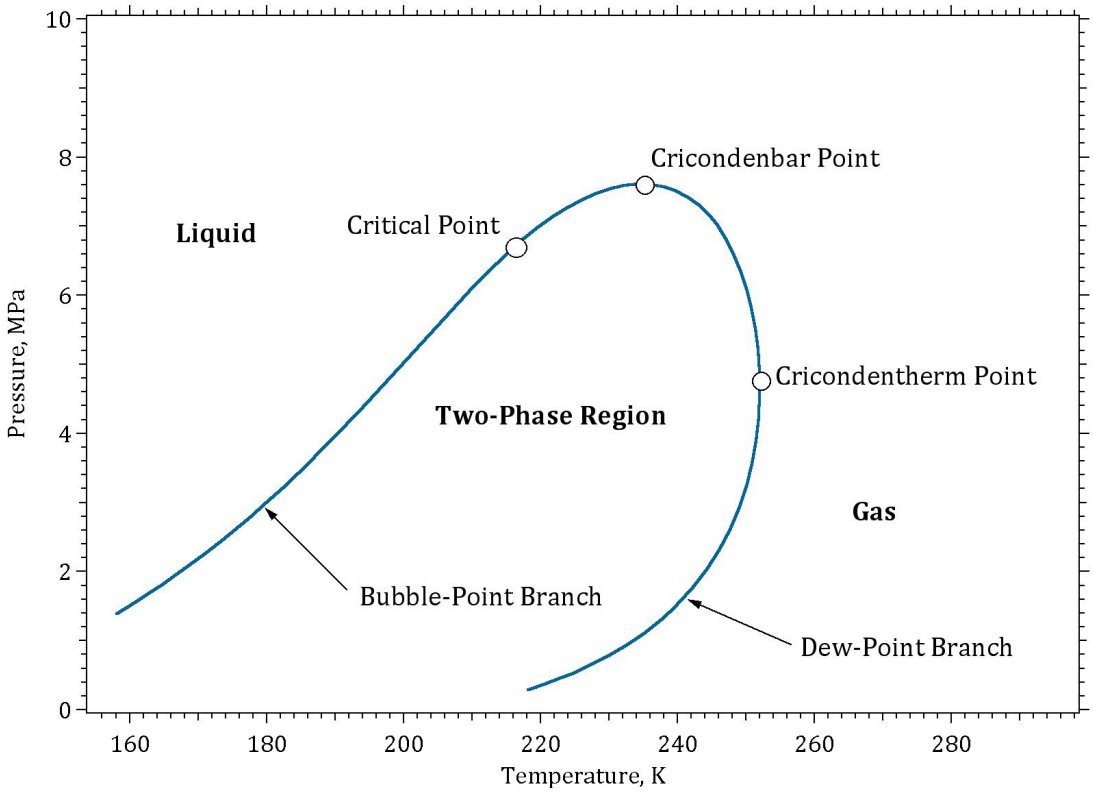

Fig. 3. Phase envelope elements (adopted from Pedersen and Christensen [30]).

4. Farnsworth Field Application

To demonstrate the application of the STOMP-EOR simulator to a field-scale problem numerical simulations were conducted of primary, secondary waterflooding, and tertiary CO_2 injection recovery of oil and gas from an existing five-spot pattern of wells in the Farnsworth Field, using the compositional option. The computational domain, porosity distribution, and intrinsic permeability distribution for the simulations were those derived from history matching simulations conducted for the primary and secondary recovery periods, as part of the SWP Phase III project investigations. The oil composition was that used in a previous optimization study of combined CO_2 sequestration and enhanced oil recovery at the Farnsworth Field [31]. The principal objective of this suite of simulations was to compare gross recovery results against field observations, and to determine the computational requirements for conducting simulations. Three separate simulations were conducted: 1) 1000-day primary recovery from all five wells, 2) 1000-day secondary recovery from a central producer with water injection in the four peripheral wells, and 3) 1000-day tertiary recovery from a central producer with an alternating water and CO_2 (WAG) injection in the four peripheral wells. The WAG schedule was not optimized, but set at 50% water injection and 50% CO_2 injection by time.

4.1. Farnsworth Field Production History

First production at the Farnsworth Field, located in Ochiltree County, Texas, USA (Anadarko Basin of northern Texas) was that of natural gas starting on May 26, 1952 [32]. Gas production continued until June 1956 with a cumulative production of 1,219,664 MCF of gas and 10,643 barrels of distillate oil [32]. Union Oil Company of California (Unocal) started oil production on July 24, 1955 [32], recovered oil from this period was 38° API gravity with at gas-to-oil ratio of 305 ft^3 gas/barrels of oil. The second Unocal field well drilled into the Pennsylvanian aged upper Marrow initially flowed 322 BOPD (barrels of oil per day) from a 3/8-in choke with a flowing tube pressure of 75-125 psi [33]. The initial bubble point pressure and formation volume fraction of the oil was 2059 psi and 1.192 BBL/BBL (barrels at surface pressure per barrel at formation depth) [34,35], respectively. The Well perforations were between 7,966-7,990 ft (2428-2435 m). The primary reservoir in the Farnsworth area is a Morrow sand with an average thickness of 29 ft (8.84 m) and maximum thickness of 54 ft (16.46 m) [32]. Upper Morrow sands vary vertically and laterally over relatively short distances from siliceous coarse-grained sands to gritty quartz conglomerates, all exhibiting strong bedding planes [32]. Primary production operations continued at the Farnsworth Field until 1965. On January 30, 1964 the application by Unocal for secondary recovery by waterflooding was approved. At the time of approval 125 wells were producing oil from the Farnsworth Field. By November of 1986 the field had produced in excess of 36 million barrels of oil, and in 1989 the field was being studied by Unocal for the potential of tertiary recovery with CO_2 injection.

As of November 1987, there were 73 active production or injection wells. In 1989 Munson [33] completed a geological study of the Farnsworth Field, using cores from 49 wells that penetrated the upper Morrow sandstone and reported an average porosity of 14.53%, intrinsic permeability of 48.2 mD, and connate water saturation of 31.4%. The actual produced oil from primary recovery activities was 9,798,640 BO (barrels of oil), which equaled 8.9% of the original oil in place (OOIP). Estimated amounts of recoverable oil via secondary waterflooding was 42,626,598 BO, which represented an additional 35.6% of OOIP (i.e., 119,552,000 BO) [33]. Cumulative production of oil and gas, as of November 30, 1986, was 36,342,520 BO and 28,779,870 MCFG (thousand cubic feet of gas). The projection for achieving the estimated amounts of oil through waterflooding in 1987 was 20.7 years, but the increasing amounts of produced water made secondary recovery operations uneconomical [33].

Chaparral Energy LLC, the nation's third-largest carbon dioxide enhanced oil recovery producer based on active projects, acquired the rights to the Farnsworth Field in 2009 and started injecting CO_2 into the field in December, 2010. Injected CO_2 is from two anthropogenic sources: 1) an Agrium fertilizer plant in Borger, Texas and 2) the Arkalon Ethanol Plant in Seward County, Kansas and is transported via pipelines, as part of the panhandle system with 172.5 miles of active CO_2 pipelines. Both the Borger and Arkalon sites have CO_2 compression and dehydration facilities. The Southwest Partnership and Chaparral Energy have selected the Marrow formation as the reservoir for

conducting scientific investigations on the utilization of CO_2 for enhanced oil recovery and the sequestration of CO_2 in depleted petroleum reservoirs. The planned net CO_2 injection rate is 0.19 MMt (million tonnes) per year or 1.0 MMt over the 5-year, 4-month project.

4.2. Primary Recovery Simulation

The primary recovery simulation involved pumping from 5 existing wells (i.e., #13-6, #13-7, #13-8, #13-10, and #13-11). The initial aqueous saturation and temperature was assumed uniform across the reservoir at 0.3 and 168˚F (75.5˚C), respectively. The initial pressure was set at 2217.7 psia (15.291 MPa) at the lowest point in the domain, with a hydrostatic pressure distribution. The oil was assumed to comprise four components (i.e., C1, C3C5, C6, and C10). The essential property parameters for the components plus CO_2 and initial molar fractions of the components are shown in Table 2, and the cubic equation of state binary interaction parameters are shown in Table 3. Production wells were modeled with a specified bottom-hole pressure that varied from 2100 psia (14.48 MPa) to 1200 psia (8.274 MPa) over the first 500 days, and then was held constant at 1200 psia (8.274 MPa). The wells were assumed to be vertical and screened across the active portion of the domain.

Table 2. Petroleum component property parameters and initial composition.

Petrol. Comp.	Initial Mole Frac.	Mol. Wt., gm/mol	Crit. Temp., ˚K	Normal Boiling Temp., ˚K	Critical Press., MPa	Critical Molar Volu., cm^3/mol	Critical Comp.	Pitzer Acentric Factor	Isobaric Specific Heat (a), J/mol K	Isobaric Specific Heat (b), J/mol K^2	Isobaric Specific Heat (c), J/mol K^3
C1	0.1	16.23	188.85	111.67	4.600	98.62	0.288	0.0114	19.25	0.0521	-1.197e-5
CO2	0.0	44.01	304.21	194.69	7.377	94.12	0.274	0.2239	19.80	0.0734	-5.602e-5
C3C5	0.05	60.70	291.20	429.5	3.628	272.36	0.2767	0.2001	190.73	-0.2091	4.175e-5
C6	0.8	134.15	436.04	641.34	2.635	665.08	0.3286	0.3827	373.95	-0.4212	9.400e-5
C10	0.05	174.94	489.81	668.35	1.854	748.72	0.2498	0.5601	489.41	-0.5500	1.220e-4

Table 3. Petroleum component binary interaction parameters.

Petroleum Component	C1	CO2	C3C5	C6	C10
C1	0.0	0.10218	0.00263	0.01078	0.0
CO2	0.10218	0.0	0.11779	0.1150	0.11
C3C5	0.00263	0.11779	0.0	0.0	0.0
C6	0.01078	0.1150	0.0	0.0	0.0
C10	0.0	0.11	0.0	0.0	0.0

Production from the five wells was not uniform, as the permeability field was heterogeneous, as shown in Fig. 4. The total produced oil over the 2500-day period for the five wells was 1,898,946 BO for an average production rate of 151.9 BOPD for each well. This compares reasonably with the 322 BOPD measured initially for the reservoir. The nonaqueous-liquid saturation did not vary greatly within the five-spot pattern during primary recovery from the initial value of 0.7, see Fig. 5, as oil was drawn into the pattern from outside and the relatively coarse grid blocks

used for the simulation. Reductions in oil saturations would be greater within the five-spot pattern had other wells been producing from the reservoir.

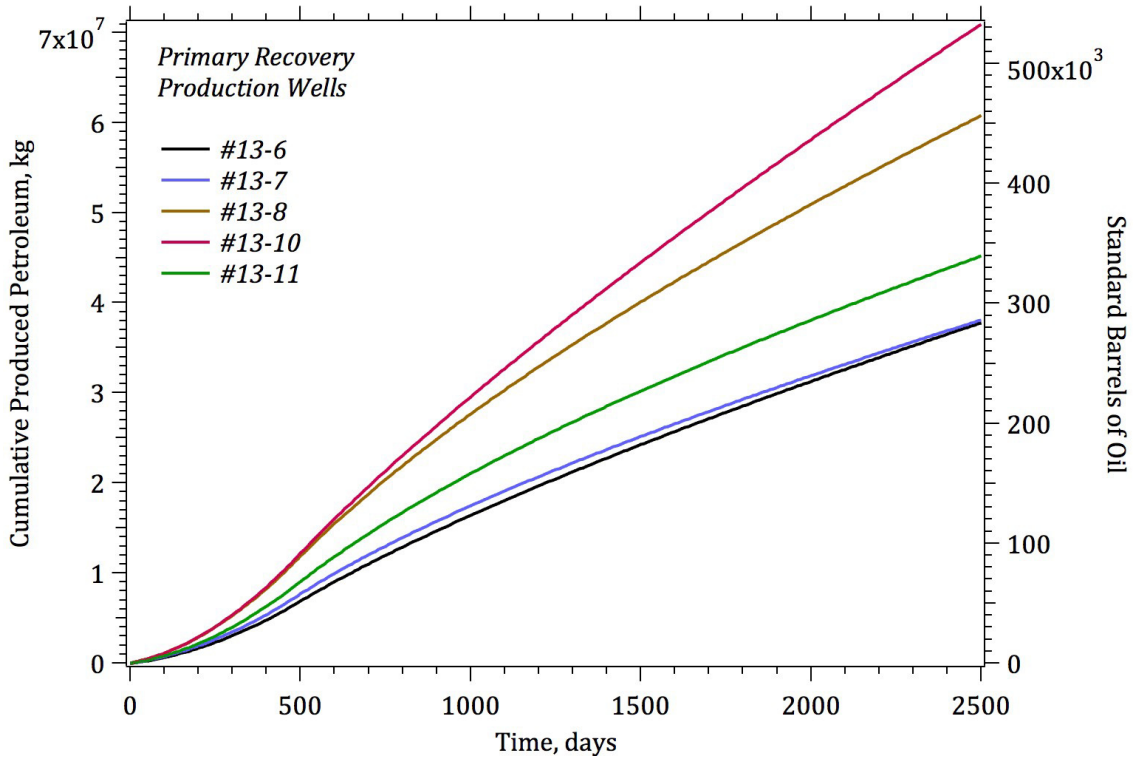

Fig. 4. Oil production during primary recovery from a five-spot pattern in the Farnsworth Unit.

4.3. Secondary Recovery Simulation

The secondary recovery simulation considered water injection into the four peripheral wells (i.e., #13-6, #13-8, #13-10, and #13-11) and fluid production from the central well (i.e., #13-7). The initial conditions for the simulations where those from the primary recovery simulation after 2500 days of pumping. Pure water was injected into the four peripheral wells at a rate of 0.2 l/s (108.7 barrels/day) per well, with an upper injection pressure at the top of the screened interval of 4500 psia (31.03 MPa). Fluids were produced from the central well using a constant pressure at the bottom of the screened interval of 2100 psia (14.48 MPa). Primary production did not yield gas saturation in the formation, so the component concentrations remained constant as those specified initially for the primary-production simulation. The injection and production wells were assumed to be active over the entire simulation period of 2500 days. Injection-well pressures rise rapidly at the start of the simulation to values between 11 and 12.5 MPa, but then follow an asymptotic rise to above 15 MPa over the 2500-day simulation period. Oil production starts around 1200 days, when the pressure at the production well exceeds 14.48 MPa. The total produced oil after 2500 days is 42,767 STB. Water was not produced during the simulation period. During 1500 and 2500 days the rate of oil production is nearly constant at 37.33 STB/day, as shown in Fig 6.

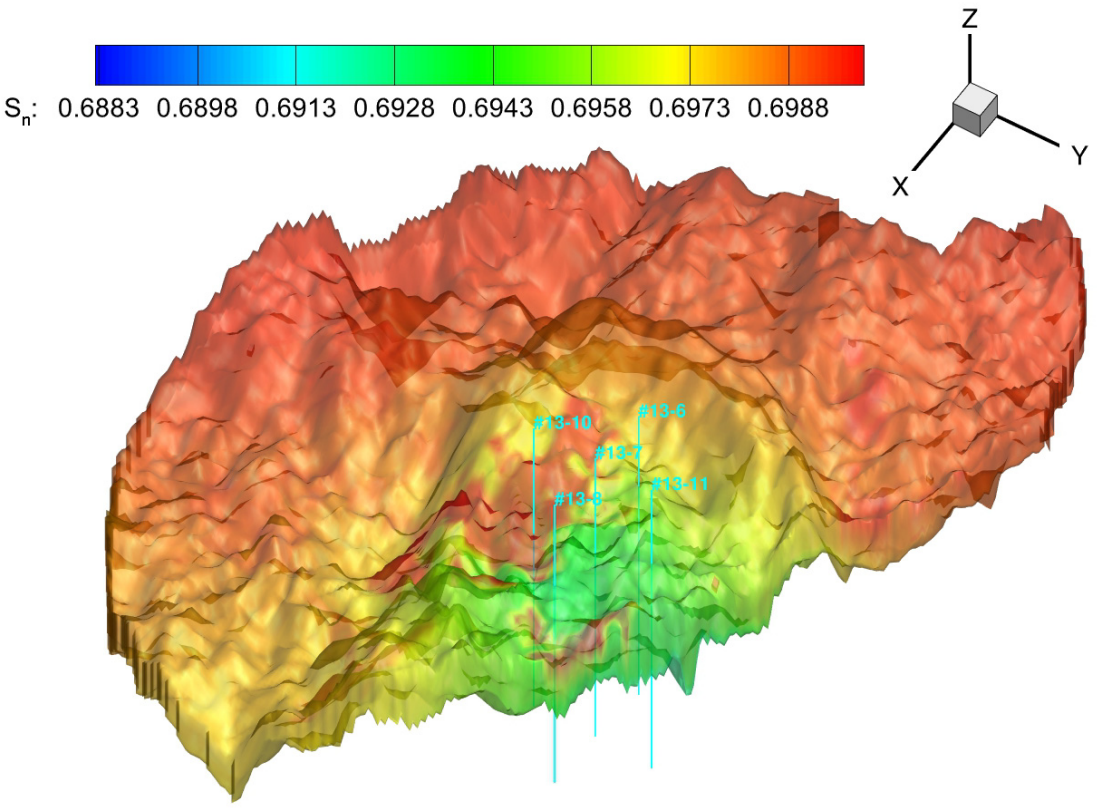

Fig. 5. Nonaqueous-liquid saturation around a five-spot pattern in the Farnsworth Unit after 2500 days of primary recovery.

4.4. Tertiary Recovery Simulation

The primary and secondary recovery simulations were principally executed to serve as initial conditions for the tertiary recovery simulation, which was the target application for this code demonstration paper. Neither primary nor secondary recovery were conducted for periods long enough to realize maximum oil recoveries, but sufficiently depleted the reservoir volume within the five-spot well pattern to initiate tertiary recovery with an alternating water and CO_2 injection cycle (i.e., WAG). The WAG cycle was identical for the four peripheral injection wells (i.e., #13-6, #13-8, #13-10, and #13-11), starting with water injection at 0.16 l/s (86.95 barrels/day) at 100˚F (37.8˚C) for 50 days and CO_2 injection at 0.3 l/s at the injection well pressure and injection temperature of 120.0˚F (48.9˚C) for 50 days. Fluid production from the central well (i.e., #13-7) was modeled using a constant pressure at the bottom of the screened interval of 4500 psia (31.03 MPa). The relatively high production pressure is specified to yield fully miscible conditions for CO_2 and oil. The Farnsworth oil has a distinctively higher than normal minimum miscibility pressure, as reported by Holm and Josendal [36]. High-pressure conditions at the production well are difficult to achieve for a single five-spot well pattern, as the reservoir volume outside of the pattern acts as a pressure sink.

The tertiary recovery simulation reveals two critical needs for accurately modeling enhanced oil recovery and CO_2 sequestration in depleted petroleum reservoirs. The first is an accurate representation of the oil composition and the second is a model for phase relative permeability in the transition between liquid and gas for pressures greater than the phase envelope. The computational time required to execute STOMP-EOR is directly dependent on the number of petroleum components used to model the oil and gas in a petroleum reservoir. Five petroleum

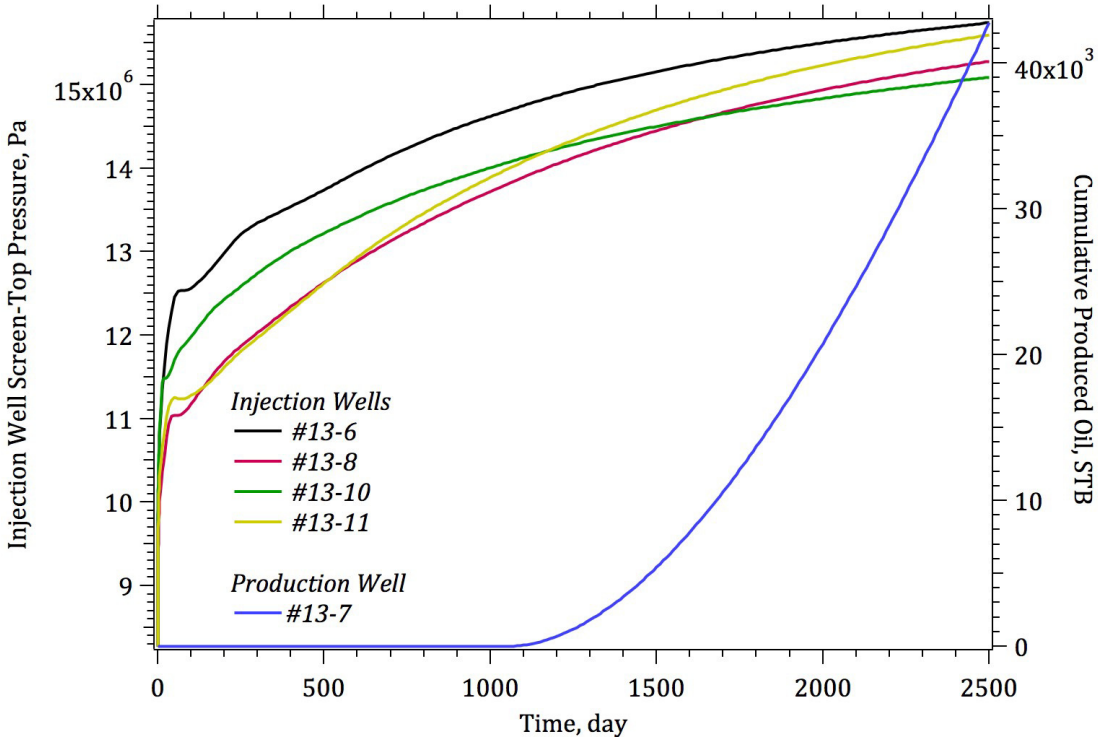

Fig. 6. Cumulative injected water and produced oil during 2500 days of secondary recovery.

components, including CO_2, were used in these demonstration simulations, but an accurate representation of the Farnsworth oil may require doubling that number. The number and characteristics of components used depends on the ability of the cubic-based equation of state to reproduce experimental PVT data, which is used to measure the volumetric and phase changes the reservoir fluid is likely to undergo from reservoir to atmospheric conditions, and within the reservoir during production, including via CO_2 injection. For example during primary recovery, reductions in reservoir pressure may yield two-phase (i.e., nonaqueous-liquid and gas) conditions. In addition to PVT properties, the compositional model must be able to yield accurate nonaqueous-liquid and gas transport properties (e.g., viscosity, thermal conductivity and diffusion coefficients) and thermodynamic properties (e.g., enthalpy, internal energy, and minimum miscibility pressure).

The aqueous and nonaqueous liquid saturations near the bottom of the CO_2 injection wells are shown in Fig. 7, for the first 500 days of the WAG schedule. The nonaqueous phase during this time period and for the specified fluid composition yields single-phase conditions above the phase envelope, indicating fully miscibility of the CO_2 with the reservoir fluid. A phase identification procedure proposed by Pedersen and Christensen [30] recommend identifying fluids with molar volume to cubic equation of state b-parameter ratio less than 1.75 as being liquid, and greater than 1.75 as being gas. To avoid flopping between liquid and gas within this region, the saturation transition function is implemented in STOMP-EOR for this single-phase region (i.e., above the phase envelope between the critical temperature and cricondentherm temperature in Fig. 3):

$$\beta = \min\left[\max\left[\left(\frac{V}{b} - 1.25\right), 0\right], 1\right] \tag{22}$$

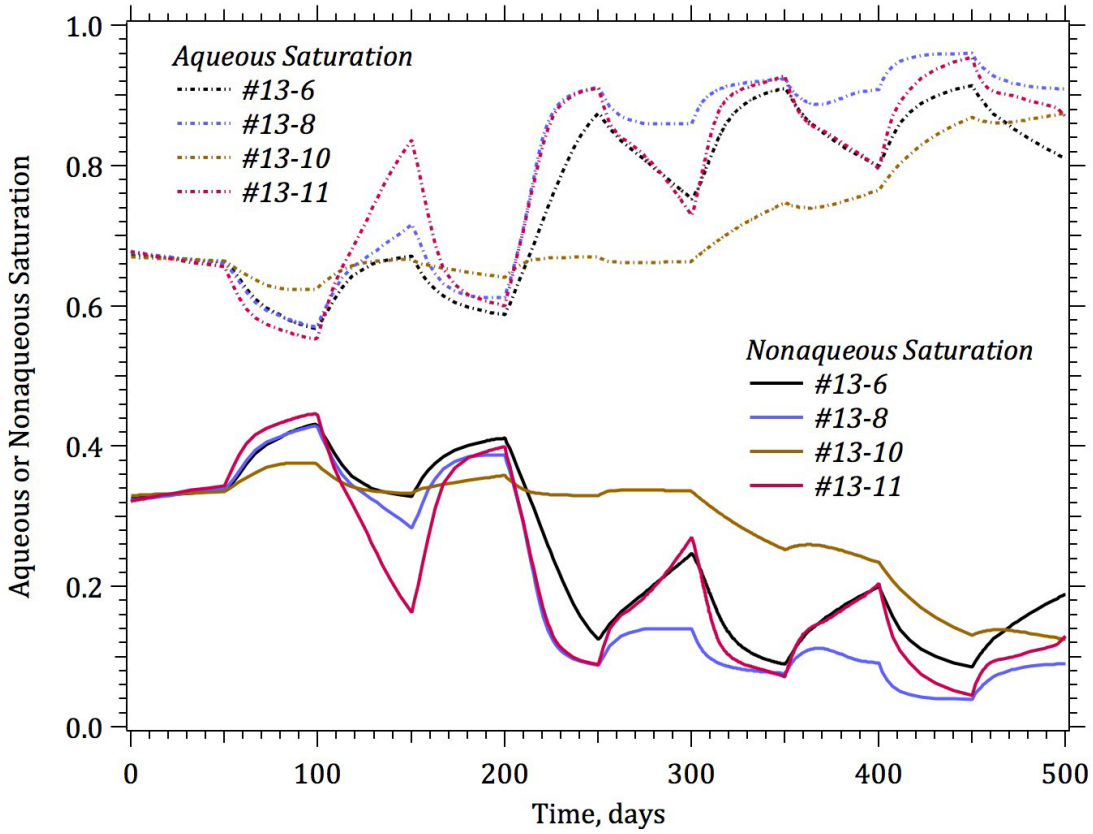

Fig. 7. Progression of aqueous and nonaqueous saturation near the four CO_2 injection wells.

where beta is the mole fraction of gas. The relative permeability of the aqueous, nonaqueous-liquid, and gas phases for petroleum reservoir modeling is generally determined from fluid-pair experiments and ternary relative permeability models, such as those developed by Stone [27,28] and Baker [29]. With CO_2 injection, however, the reservoir nonaqueous fluid often exists in the transition region between single-phase liquid and single-phase gas, which is outside of the applicable range for the models of Stone [27,28] and Baker [29]. To visualize the reservoir pressure build-up and extent of the injected CO_2 after 500 days of the WAG schedule a color-scaled and iso-surface image is shown in Fig. 8.

5. Discussion

A new numerical simulator has been developed for scientific investigations of CO_2 utilization for enhanced oil recovery and sequestration in depleted petroleum reservoirs. This simulator, STOMP-EOR, solves coupled conservation equations for energy, water mass, CO_2 mass, CH_4 mass, salt mass, and n-petroleum component mass in variably saturated geologic media with three mobile phases: 1) aqueous, 2) nonaqueous liquid, and 3) gas. The simulator was designed to solve problems concerned with the production of oil and gas from petroleum reservoirs through multiple stages of production: 1) primary (i.e., pumping of reservoir fluids), 2) secondary (i.e., waterflooding), and 3) tertiary (i.e., water alternating gas with CO_2 injection); and the sequestration of greenhouse gases in depleted petroleum reservoirs. The simulator specifically has been developed with features for conducting scientific research: 1) open source coding, 2) mixed wetting s-P functions, and 3) single-phase k-s transition model.

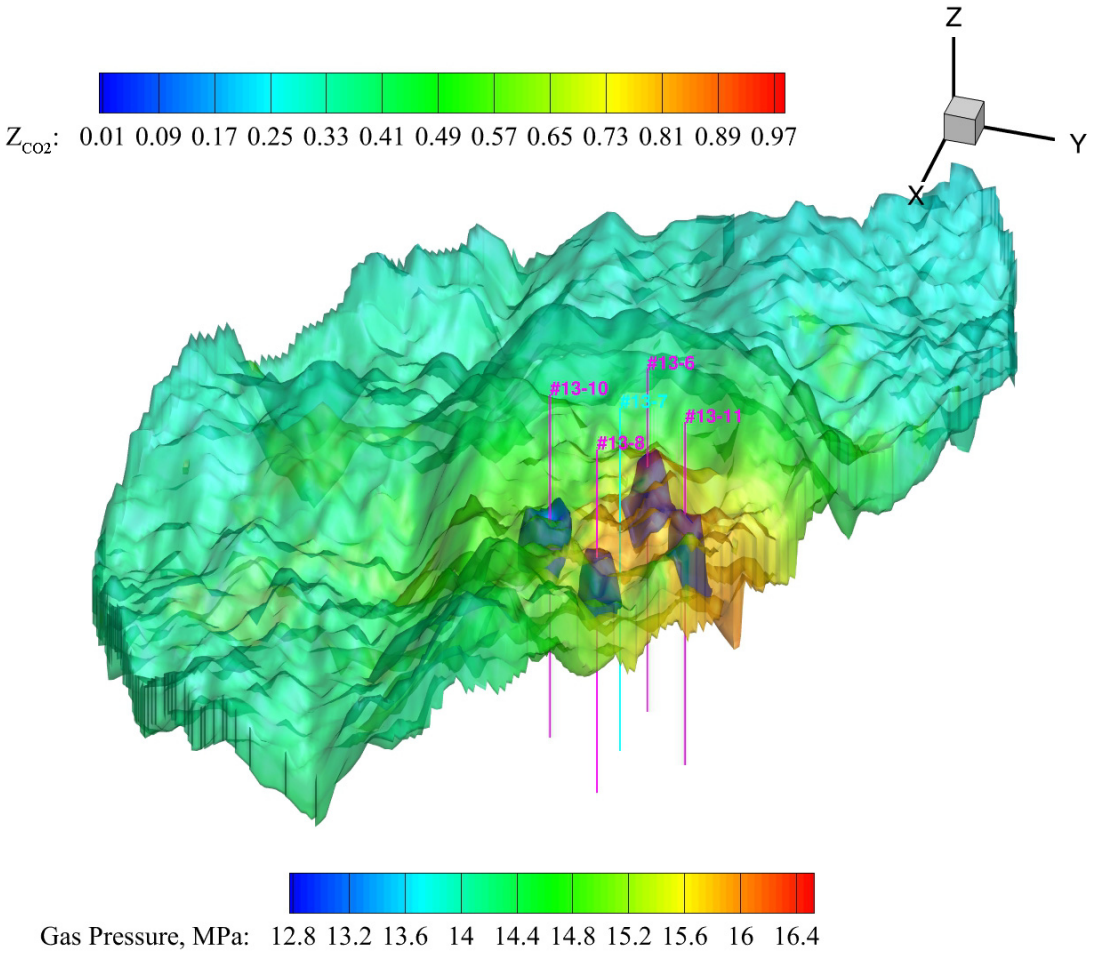

Fig. 8. Color-scale reservoir pressure and iso-surface of CO_2 extent after 500 days of the WAG schedule.

The principal objective for developing the simulator is to provide analytical tools to the scientific community for better understanding the utilization of CO_2 in enhanced oil recovery and the ultimate fate of CO_2 in depleted petroleum reservoirs. The Southwest Regional Partnership on Carbon Sequestration (SWP) Phase III Project will provide the needed geologic characterization and experimental observational data, to make it possible to use thesimulator to investigate production and sequestration scenarios, and new models for phase relative permeability across the three phases of oil recovery and CO_2 sequestration.

Sequestering greenhouse gases in deep saline reservoirs generally yields the creation of a CO_2-rich phase (e.g., supercritical CO_2 phase) and subsequent migration of that phase through the reservoir under pressure gradients and buoyancy driving forces. CO_2 becomes trapped in deep saline reservoirs via dissolution into the aqueous phase, low-permeability and high-entry-pressure structural barriers, formation of immobile CO_2-rich phase ganglia with imbibition of wetting fluids (i.e., aqueous phase), and reaction of the formation minerals to form carbonates. Numerical simulators for carbon sequestration in deep saline reservoirs have been continually advancing since around the new millennium and the current state of simulation capabilities include those for modeling the four

trapping mechanisms. The coupled thermal, hydrologic, and thermodynamic processes associated with injecting CO_2 into petroleum reservoirs for utilization in oil and gas recovery and sequestration, however, are significantly different from those in deep saline reservoirs mainly because of the range of miscibility of CO_2 with the petroleum components as a function of temperature, pressure, and oil composition. The objective behind developing the STOMP-EOR simulator has been to provide a flexible tool for investigating and understanding the rather complex coupled processes that occur with the injection of CO_2 into petroleum reservoirs. Geologic heterogeneity remains a challenge for modeling carbon sequestration in deep saline reservoirs. This challenge is compounded by heterogeneities in fluid equilibria that occur across a petroleum reservoir with the injection of CO_2. We seek to combine detailed experimental observations from the Farnsworth Unit during tertiary recovery activities by Chaparral Energy with numerical simulations to provide new insights to these complex processes, in particular fluid phase relative permeabilities.

Acknowledgements

This research has been accomplished and funded by the U.S. Department of Energy's National Energy Technology Laboratory through the Southwest Regional Partnership on Carbon Sequestration (SWP) Phase III Project with the collaboration of Chaparral Energy and the technical support of the SWP partners.

References

[1] Pruess, K, J Garcia, T. Kovscek, C Oldenburg, J Rutqvist, C Steefel, and T Xu. 2004. "Code intercomparison builds confidence in numerical simulation models for geologic disposal of CO_2." *Energy Procedia*, 29:1431-1444.

[2] Class, H, A Ebigbo, R Helmig, HK Dahle, JM Nordbotten, MA Celia, P Audigane, M Darcis, J Ennis-King, Y Fan, B Flemisch, SE Gasda, M Jin, S Krug, D Labregere, AN Beni, RJ Pawar, A Sbai, SG Thomas, L Trenty, L Wei. 2009. "A benchmark study on problems related to CO_2 storage in geologic formations." *Computational Geosciences*, 13:409-434.

[3] Mukhopadhyay, S, JT Birkholzer, J-P Nicot, and SA Hosseini. 2011. "A model comparison initiative for CO_2 injection field test: an introduction to Sim-SEQ." *Environmental Earth Sciences*, 67(2):601-611.

[4] Aziz, K, and A Settari. 1979. *Petroleum Reservoir Simulation*, Applied Science Publishers.

[5] Lim, MT, SA Khan, K Sepehrnoori, and GA Pope. 1992. "Simulation of carbon dioxide flooding using horizontal wells." In proceedings of SPE Annual Technical Conference and Exhibition, 4-7 October, Washington, D.C ., SPE-24929-MS, Society of Petroleum Engineers.

[6] tNavigator, Rock Flow Dynamics, Available from <http://www.rfdyn.com/technology> [28 July 2014].

[7] GEM, Computer Modeling Group LTD, Available from <http://www.cmgl.ca/software/soft-gem> [28 July 2014].

[8] ECLIPSE, Schlumberger, Available from <http://www.software.slb.com/products/foundation/Pages/eclipse.aspx> [28 July 2014].

[9] Nexus, Landmark, Halliburton, Available from <http://www.landmarksoftware.com/Pages/Nexus.aspx> [28 July 2014].

[10] The Southwest Partnership, Available from <http://www.southwestcarbonpartnership.org> [28 July 2014].

[11] Chaparral Energy, Available from <http://www.chaparralenergy.com> [28 July 2014].

[12] Spycher, N, K Pruess, and J Ennis-King. 2003. "CO2-H2O mixtures in geological sequestration of CO2. I. Assessment and calculation of mutual solubilities from 12 to 100˚C and up to 600 bar." *Geochimica et Cosmoschimica Acta*, 67(16):3015-3031, doi:10.1016/s0016-7037(03)00273-4.

[13] Spycher, N and K Pruess. 2010. "A phase-partitioning model for CO2-brine mixtures at elevated temperatures and pressures: Application to CO2-enhanced geothermal systems." *Transport in Porous Media*, 82:173-196, doi:10.1007/s11242-009-9425-y.

[14] Meyer, CA, RB McClintock, GJ Silvestri, and RC Spencer. 1993. *ASME Steam Tables*, The American Society of Mechanical Engineers, New York.

[15] Peng, D-Y, and DB Robinson. 1976. "A new two-constant equation of state." *Ind. Eng. Chem. Fundam.*, 15:59-64.

[16] Redlich, O and JNS. Kowg. 1949. "On the thermodynamics of solutions." *Chem. Rev.*, 44:233-244.

[17] Soave, G. 1972. "Equilibrium constants from a modified Redlich-Kwong equation of state." *Chem. Eng. Sci.*, 27:1197-1203.

[18] Peneloux, A, E Rauzy, and R Fréze. 1982. "A consistent correction of Redlich-Kwong-Soave volumes." *Fluid Phase Equilibria*, 8:7-23.

[19] Michelsen, ML and JM Mollerup. 2007. *Thermodynamic Models: Fundamentals & Computational Aspects*, Second Edition, Tie-Line Publications, Holte, Denmark, ISBN 87-989961-3-4.

[20] Wilson, GM 1969. "A modified Redlich-Kwong equation of state. Application to general physical data calculation." Paper No. 15C presented at the *1969 AIChE 65th National Meeting*. Cleveland, OH, March 4-7, 1969.

[21] Rachford, HH Jr. and JD Rice. 1952. "Procedure for use of electronic digital computers in calculating flash vaporization hydrocarbon equilibrium." *Journal Petroleum Technology*, 4.

[22] van Genuchten, MTh. 1980. "A closed-form equation for predicting the hydraulic conductivity of unsaturated soils." *Soil Science Society of America Journal*, 44:892-898.

[23] Brooks, RH and AT Corey. 1964. "Hydraulic properties of porous media," *Hydraulic Paper No. 3*, Colorado State University, 1964.

[24] Webb, SW, 2000. "A simple extension of two-phase characteristic curves to include the dry region." *Water Resources Research*, 36(6):1425-1430.

[25] Bennion, B, and S Bachu. 2005. "Relative permeability characteristics for supercritical CO_2 displacing water in a variety of potential sequestration zones in the Western Canada Sedimentary Basin. Society of Petroleum Engineers, SPE 95547, In proceedings of 2005 SPE Annual Technical Conference and Exhibition held in Dallas, Texas, USA, 9-12 October 2005.

[26] Juanes, R, EJ Spiten, FM Orr Jr, and MJ Blunt. 2006. "Impact of relative permeability hysteresis on geological CO_2 storage." *Water Resources Research*, 42:W12418, doi:10.1029/2005WR004806.

[27] Stone, HL. 1970. "Probability model for estimating three-phase relative permeability." *Journal of Petroleum Technology*, 22(2):214–218. SPE-2116-PA. http://dx.doi.org/10.2118/2116-PA.

[28] Stone, HL. 1973. "Estimation of three-phase relative permeability and residual oil data." *Journal of Canadian Petroleum Technology*, 12(4):53-61. http://dx.doi.org/10.2118/73-04-06.

[29] Baker, LE. 1988. "Three-phase relative permeability correlations." Presented at the SPE Enhanced Oil Recovery Symposium, Tulsa, Oklahoma, 16-21 April 1988. SPE-17369-MS. http://dx.doi.org/10.2118/17369-MS.

[30] Pedersen, KS and PL Christensen. 2007. *Phase Behavior of Petroleum Reservoir Fluids*, CRC Press, ISBN 0-8247-0694-3.

[31] Dai, Z, R Middleton, H Viwanathan, J Fessenden-Rahn, J Bauman, R Pawar, S-Y Lee, and B McPherson. 2014. "An integrated framework for optimizing CO_2 sequestration and enhancing oil recovery." *Environmental Science and Technology Letters*, 1:49-54, American Chemical Society, dx.doi.org/10.1021/ez4001033.

[32] Parker, RL. 1956. "Farnsworth Morrow Oil Field." *The Panhandle Geonews*, 4(1):5-12.
Available from <http://archives.datapages.com/data/index.html> [30 July 2014]

[33] Munson, TW. 1989. "Depositional, diagenetic, and production history of the Upper Morrow Buckhaults Sandstone, Farnsworth Field, Ochiltree County Texas." *The Shale Shaker Digest*, July/August 1989.
Available from <http://archives.datapages.com/data/index.html> [30 July 2014]

[34] May, RS. 1987. "A numerical simulation study of the Farnsworth Unit Waterflood (West Side)." Science and Technology Project Report 87-32, Unocal Corporation, Unocal Science and Technology Division, Brea, California.

[35] Hinds, RF. 1956. "Reservoir Fluid Study, Messall No. 2 Well, Farnsworth (Upper Morrow) Field, Ochiltree County, Texas." Core Laboratories, Inc, Petroleum Reservoir Engineering, Dallas, Texas.

[36] Holm, LW, and VA Josendal. 1980. "Effect of oil composition on miscible-type displacement by carbon dioxide." SPE-8814, In proceedings of First Joint Symposium on Enhanced Oil Recovery, Tulsa, Oklahoma, April 20-23, 1980, Society of Petroleum Engineers.